Analysis of the electron excitation spectra in heavy rare earth metals, hydrides and oxides

C. Colliex, M. Gasgnier, P. Trebbia

Classification
Physics Abstracts
2.820 — 8.800 — 8.120

ANALYSIS OF THE ELECTRON EXCITATION SPECTRA IN HEAVY RARE EARTH METALS, HYDRIDES AND OXIDES

C. COLLIEX (*), M. GASGNIER (**), P. TREBBIA (*)

(*Reçu le 6 octobre 1975, révisé le 27 novembre 1975, accepté le 22 décembre 1975*)

Résumé. — Les spectres de pertes d'énergie d'électrons de 75 keV à travers des couches minces évaporées de terres rares lourdes (Gd, Tb, Dy, Ho, Er, Tm, Yb, Lu) dans trois états chimiques différents (métal, hydrure, oxyde) sont composés essentiellement de deux pics dus aux excitations collectives (plasmons) entre 10 et 17 eV et aux excitations d'électrons 5p entre 30 et 40 eV. Une analyse quantitative de la distribution spectrale des intensités nous permet de calculer la fonction perte d'énergie et, par l'intermédiaire d'une transformation de Kramers-Krönig, la constante diélectrique et la force d'oscillateur dipolaire. Les différents résultats sont interprétés en termes de structure de bandes, ce qui nous conduit à proposer un modèle simple pour les transitions interbandes observées dans les oxydes.

Abstract. — The energy loss spectra of 75 keV electrons transmitted through thin evaporated foils of heavy rare earths (Gd, Tb, Dy, Ho, Er, Tm, Yb, Lu) in three different chemical states (metal, hydride and oxide) exhibit two main peaks due to collective « plasmon » excitations in the 10-17 eV energy range and to inner 5p excitations between 30 and 40 eV. A quantitative analysis of the intensity spectral distribution allows one to calculate the energy loss function and, through a Kramers-Krönig inversion, the dielectric constant and the dipole oscillator strength. Various results are then explained in terms of band structure, so that we are lead to propose a simple model for the interband transitions occuring in oxides.

1. **Introduction.** — Among the various techniques which allow the study of the electron excitation spectra in solids, the energy loss spectroscopy of electrons transmitted through thin foils has revealed some advantages and some limitations. When combined with an electron microscope, we proved in previous studies [1] that the measurement could be achieved on reduced areas and this possibility is quite useful in highly reactive materials where chemical transformations can expand in localized parts of the specimen. The registration of the energy loss spectrum over a wide range of energy (0-100 eV or more) in a single sweep is also very useful because it reduces the uncertainties in the extrapolation procedures at high frequency which are amenable to errors in a Kramers-Krönig inversion. On the other hand, the energy resolution is not high enough in the low energy region (*visible domain*) to exhibit the excitation spectrum of the conduction electrons near the Fermi level : moreover, these individual excitations, either intraband or interband, are generally hidden by collective effects in the moderate energy range (5 to 20 eV) where they are quite interesting.

The purpose of this paper is to present our experimental results concerning the electron energy loss spectra of high energy incident electrons (75 keV) transmitted through thin foils of yttric rare earth elements (gadolinium to lutetium in the periodic classification) prepared in various chemical states (metal, hydride and oxide) and which have been previously checked by standard X-ray and electron diffraction techniques.

These materials have been the subject of relatively few experimental studies leading to the determination of their electron excitation spectra. Optical measurements have been achieved for a photon energy range extending at the maximum to 12 eV [2] while characteristic energy loss measurements were performed on some of these materials. Bakulin *et al.* [3] checked the evolution of the spectra during the oxidation process due to the heating by the electron beam and Daniels [4] has extracted from his results the optical constants of Gd and Dy between 0 and 50 eV.

In a preliminary note [5] we have shown the extent to which the recorded spectra are sensitive to the chemical state of the sample during observation « in vacuo » using the electron microscope, by comparing microdensitometer traces of energy loss spectra registered on small areas of about 1 μ^2 of dysprosium metal, hydride and oxide. A similar study has also been achieved for scandium and yttrium [6] where

(*) Laboratoire de Physique des Solides associé au C.N.R.S., Université Paris-Sud, 91405 Orsay, France.
(**) Laboratoire des Terres Rares, C.N.R.S., 92-Bellevue, France.

we could select characteristic metallic spectra to perform the calculation of various dielectric or optical parameters.

In fact, because of their external electron configuration ($5d^1\ 6s^2$), the heavy rare earth materials (which are the goal of the present investigation) are expected to exhibit rather similar excitation spectra to those observed in scandium and yttrium. Any differences, if they exist, must reveal the influence of the localized 4f states. We shall check that except for ytterbium, which becomes divalent in the metal state with a filled 4f-electron shell, this influence remains weak. We have also extended our analysis of the experimental data to the conducting hydrides and the insulating oxides to determine how band structure is modified by the presence of extra electrons brought by the hydrogen or oxygen atoms. The comparison with calculated band model is necessarily limited because of the lack of results in this field.

2. **Experimental technique and results.** — Metal foils of thickness between 500 and 1 000 Å are prepared by vacuum evaporation from bulk material of standard purity (99 %) or high purity (99.95 %) in a vacuum of the order of a few 10^{-6} torr. As these metals act as very efficient getters (especially for residual hydrogen), the vacuum becomes better (the pressure decreases) as the evaporation procedes. Under these conditions, thin foils generally display two crystal structures : an hcp structure for the microcrystallised metal phase and a fcc structure for larger crystals of an hydride LnH_x phase with x of the order of 2 [7]. Although it may be possible to achieve more specific measurements on these larger crystals, it must be borne in mind that the very small size (of the order of hundred angströms) of the metal grains allows the trapping of various impurities along the numerous grain boundaries. This leads to a rather high contamination rate which cannot be detected by diffraction techniques. The situation is slightly different for ytterbium thin films : they exhibit an extra system of diffraction lines corresponding to an fcc phase with $a = 4.87$ Å, which does not seem to be an hydride but a more complex phase (YbO or Yb_2OC).

An *in situ* heating of the specimen with the electron beam induces recrystallisation processes leading to the occurrence of large crystals of sesquioxides Ln_2O_3 : the structure is generally cubic (bcc) corresponding to the phase labelled C. But the Gd_2O_3 and Tb_2O_3 thin foils that we have observed exhibit a type B monoclinic structure. The atomic density in these two structures however remains nearly equal.

These samples are then observed with a conventional transmission electron microscope fitted with a Castaing and Henry type dispersive unit. This system allows one to select a given area of the sample of a size of the order of 0.2 μm × 0.2 μm by means of an aperture and to register the energy loss spectrum corresponding to this volume of material.

It has been clearly established that this technique could be used for microanalytical purposes when one looks at the more characteristic lines at higher energy losses [8]. In the following however, we shall focus our attention on the excitation processes which appear in the moderate energy range (0 to 50 eV) of the spectra. An example of such a family of experimental spectra is displayed in figure 1. This example clearly shows the limits of this method of selection : the *metal* curve A exhibits a strong plasmon peak at 10 eV and a *oxide* weak bump at 18 eV, but in the curve B the relative importance of these two features

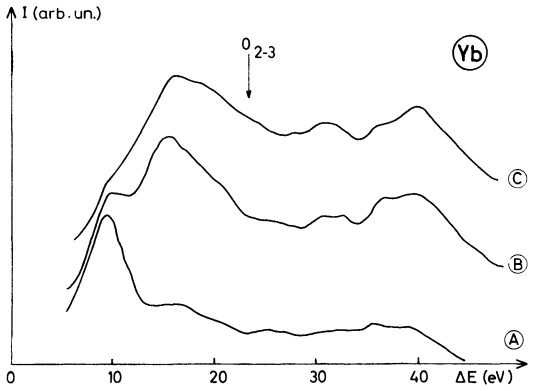

FIG. 1. — Experimental electron energy loss spectra of 75 keV through thin films of : metallic ytterbium (A) ; YbO or Yb_2OC (B) ; Yb_2O_3 (C). $O_{2\,3}$ threshold, as given by Bearden and Burr [20], is located by the arrow.

is reversed. It must be admitted that neither of these two spectra is typical of one (or the other) of the two phases (metal or oxide) but that they are representative of a mixture of them in reversed concentrations. A more detailed analysis of the intensity distribution of these spectra in terms of the dielectric constant would therefore be meaningless because of their lack of representativity of a well reproducible phase. Nevertheless, the position of the peaks is less sensitive to these compositional variations and in a first approach, these results can be discussed qualitatively within the framework of a free electron model. Table I summarises our results for the location of the peaks for a great number of spectra. This table exhibits only slight discrepancies with the results which have been already published in reference [5], but is more complete with respect to the oxides.

Except for the special case of ytterbium which we have already mentioned, these spectra display the following general features : a main peak (A) around 15 eV due to collective excitations of the upper electron band ; one or several weak structures and a second important peak (B) between 30 and 40 eV which must be associated with the excitation of the 5p electrons of the metal atom.

We have deliberately omitted the characteristic lines appearing at much higher energies (around

TABLE I

Experimental values (eV) *of peak A* (± 0.3 eV) *and peak B* (± 0.5 eV) *position in electron energy loss spectra for different chemical states of thin evaporated layers of lanthanides*

	Metal Ln		Hydride LnH_2		Oxide Ln_2O_3		O_{II-III} threshold (20)
	A	*B*	*A*	*B*	*A*	*B*	
	—	—	—	—	—	—	—
Gd	14.2	34.7	16.3	35.0	14.5	36.0	20.3
Tb	13.3	35.5	15.6	35.5	14.8	36.2	25.4
Dy	14.0	36.5	16.9	36.5	15.6	37.2	26.3
Ho	13.5	37.0	16.5	37.2	15.8	37.8	20.3
Er	14.0	38.0	16.8	38.0	15.0	38.4	29.4
Tm	14.3	39.0	17.0	39.3	15.6	39.3	32.3
Lu	14.9	41.0	17.2	42.0	16.7	42.0	28.0

Yb		YbO or Yb_2OC		Yb_2O_3		$O_{II\ III}$ (20)
A	*B*	*A*	*B*	*A*	*B*	
—	—	—	—	—	—	—
9.7	39.0	16.7	39.5	17.0	40.0	23.4

150 eV) which are due to the excitation of 4d electrons as we have discussed previously [9].

3. **Determination of the energy loss function and optical constants.** — An energy loss spectrum is a representation of the spectral distribution of the energy loss function $-\operatorname{Im}\frac{1}{\varepsilon(\omega)}$, which expresses the causal response of the medium to the disturbing external electron charge carried in the electron beam. It can be related to the function $\operatorname{Re}\frac{1}{\varepsilon(\omega)}$ by means of the well-known Kramers-Krönig integral and from there, it is possible to calculate the standard coefficients ε_1, ε_2 and other related optical parameters. Such an approach is necessary in order to extend the interpretation beyond the simplified free electron model and to reveal some density of states effects.

We have therefore selected a few very representative spectra to which we have applied the following succession of operations, which constitute a simplified version of the quantitative analysis method of energy loss spectra described by Wehenkel [10].

3.1. The experimental data are recorded photographically and then analysed with a microdensitometer trace. In order to avoid the non-linearity limitation which occurs at high optical density D, we have retained only the profiles which exhibit interesting features (plasmon-peaks...) between $D = 1$ and 2. Saturation effects can however be observed on the elastic peak and several estimations of its magnitude have been tested during the procedure of deconvolution of multiple scattering events. The substraction of the elastic peak is accompanied by an extrapolation of the energy loss profile at low energies. This is responsible of the major source of error in our analysis of the data. For the metallic samples we assume a linear extrapolation to zero, and for the insulating oxide we assume a band gap of 3 eV which seems reasonable in comparison to other insulating transition oxides such as TiO_2 and V_2O_5. It must be therefore remembered that the structures which appear below 5 eV (for the following calculations) must be regarded with skepticism. The intensity spectral distribution is then digitalised with a one eV step which is sufficient because these spectra exhibit always rather large structures.

3.2. The experimental spectrum (ES) which is now expressed in arbitrary units, is subjected to a simplified multiple loss deconvolution procedure. By integration from $\Delta E = 1$ eV, we compute :

$$\mathrm{DS}(\Delta E) = \frac{1}{2 I_0}\psi(\theta_{\Delta E}) \times \times \int_0^{\Delta E} \mathrm{ES}(\Delta E_1).\mathrm{ES}(\Delta E - \Delta E_1)\, \mathrm{d}\,\Delta E_1$$

where I_0 is the elastic peak signal, $\psi(\theta_{\Delta E})$ is a parameter which describes the angular correlations in the successive scattering events and remains of the order of 1 as long as $\Delta E < 100$ eV. We can by a similar procedure also calculate a triple scattering contribution TS, and so on... By substraction, we then determine an approximate estimation of the single event profile $I_1(\Delta E)$. We have at this level of approximation neglected the surface excitation contribution which remains weak for such specimen thicknesses. Figure 2 shows an example of this procedure applied to terbium.

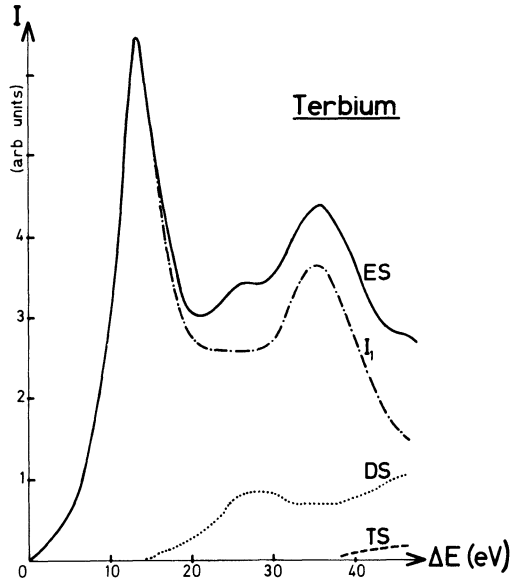

FIG. 2. — Energy loss spectrum of Terbium (ES) expressed in arbitrary units, with its single loss (I_1), double loss (DS), triple loss (TS) components.

3.3. The energy loss function $-\operatorname{Im}\frac{1}{\varepsilon}$ is then calculated after division by the function $F_\theta(\Delta E)$ introduced by Keil [11]. The latter function describes the angular distribution of the inelastically scattered electrons. The beam geometry in our experimental arrangement corresponds to an illuminating divergence angle $\theta_i \sim 10^{-3}$ rad or less, which remains much smaller than the maximum angle of collection θ_{max} equal to 5×10^{-3} rad, defined by the contrast aperture in the back focal plane of the objective lens. The geometrical arrangement described by Wehenkel [10] corresponds to the situation generally encountered in the scanning transmission electron microscope (STEM), which is similar to ours as a consequence of the reciprocity theorem. The function can therefore be evaluated in a similar way and one finds

$$F(\Delta E) = 2\pi \int_0^{\theta_{max}} \frac{\theta \, d\theta}{\theta^2 + \theta_{\Delta E}^2} = \pi \operatorname{Log}\left(1 + \frac{\theta_{max}^2}{\theta_{\Delta E}^2}\right)$$

where

$$\theta_{\Delta E} = \frac{\Delta E}{2 E_0}$$

and E_0 is the primary energy.

The energy loss function is then normalized as in reference [6] by using the well-known sum rule :

$$\operatorname{Re}\frac{1}{\varepsilon(0)} = 1 - \frac{2}{\pi}\int_0^{\infty} \operatorname{Im} -\frac{1}{\varepsilon(\Delta E)} \cdot \frac{d(\Delta E)}{\Delta E}.$$

For the metallic samples, $\operatorname{Re}\frac{1}{\varepsilon(0)} = 0$, but the situation is slightly different in the oxide situation ; as we could not find any precise determination of $\varepsilon(0)$ in the literature, we assumed it to be of the order of 10 in Dy_2O_3. Actually, a rather large uncertainty in the value of $\varepsilon(0)$ involves only a moderate variation of the intensities of the energy loss function. Moreover, it does not seem worthwhile to try to determine the thickness of the sample with an improved accuracy because, during the recrystallisation process, the thickness of the *in situ* grown oxide crystals is not uniform at all. The thinner parts are located on

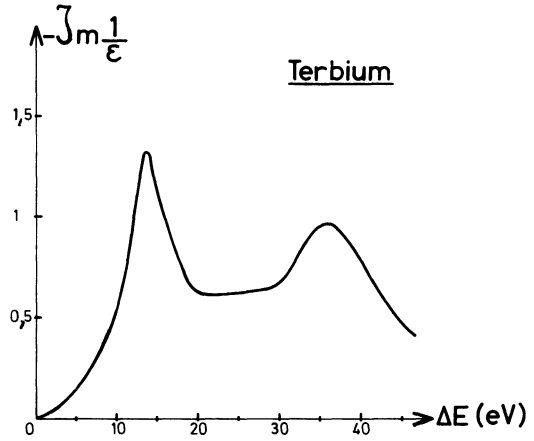

FIG. 3. — Energy loss function of Tb.

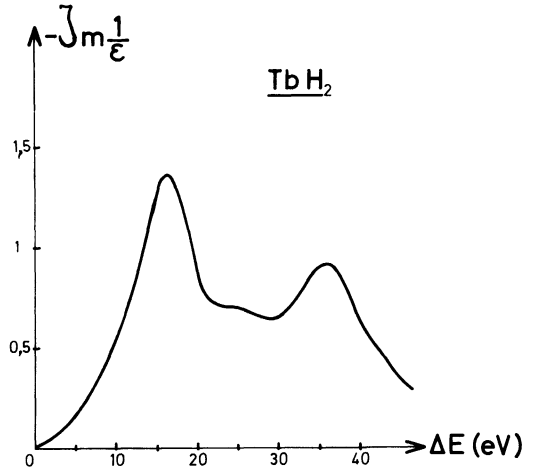

FIG. 4. — Energy loss function of TbH_2.

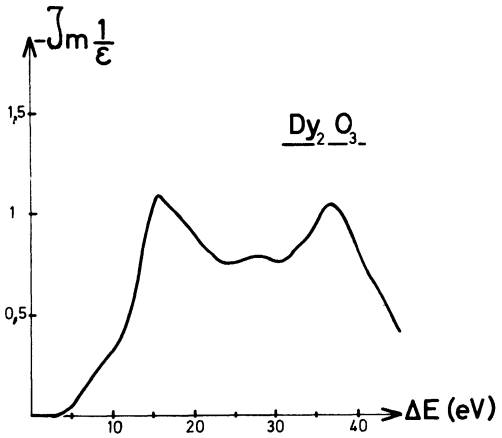

FIG. 5. — Energy loss function of Dy_2O_3.

the grain boundaries as can be deduced from the visibility of typical bend contours and thickness fringes contrasts.

The results of our determination of the energy loss function $-\operatorname{Im}\frac{1}{\varepsilon(\Delta E)}$ for the metal terbium, the hydride TbH_2 and the oxide Dy_2O_3 are shown in figures 3, 4 and 5.

3.4. The Kramers-Krönig inversion formula is then used to derive $\operatorname{Re}\frac{1}{\varepsilon(\Delta E)}$

$$\operatorname{Re}\frac{1}{\varepsilon(\Delta E)} = 1 - \frac{2}{\pi}\int_0^\infty \frac{\operatorname{Im} -\frac{1}{\varepsilon(\Delta E')}}{\Delta E'^2 - \Delta E^2}\,\Delta E'\,\mathrm{d}\,\Delta E'$$

and from there, $\varepsilon_1(\Delta E)$ and $\varepsilon_2(\Delta E)$ the real and imaginary parts of the dielectric constant. The extrapolation procedure of $\operatorname{Im} -\frac{1}{\varepsilon(\Delta E')}$ towards high energy losses is not very critical because no important structure appears above 50 eV; the decrease behaves as $\Delta E^{-\gamma}$ (where γ is of the order of 2 to 3), but the total contribution of this part of the spectrum in the inversion procedure remains weak. The results of our calculations of ε_1 and ε_2 for terbium, terbium hybride and dysprosium oxide are gathered in figures 6, 7 and 8. In order to make reference to optical measurements which may be carried out on similar samples, we have also chosen to compute $\mathrm{d}f/\mathrm{d}(\Delta E)$ which represents the density of oscillator strengths which can be excited in a dipolar transition. This quantity, proportional to $\Delta E.\varepsilon_2(\Delta E)$, is directly

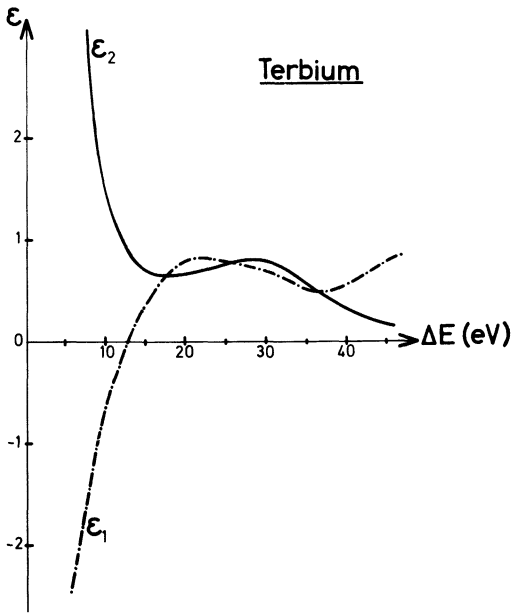

FIG. 6. — Dielectric constant ε of Tb.

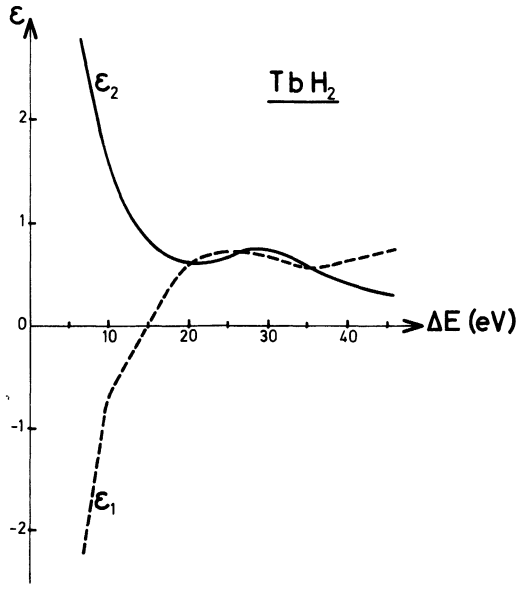

FIG. 7. — Dielectric constant ε of TbH_2.

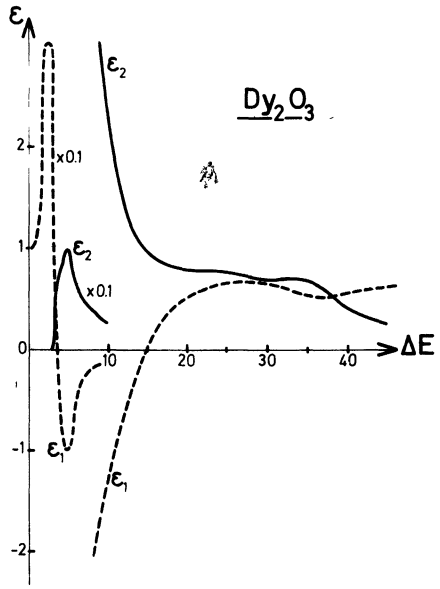

FIG. 8. — Dielectric constant ε of Dy_2O_3.

connected to the interaction process between the photon field and the electron distribution in the solid. Results are shown in figures 9, 10 and 11. Finally, we have computed the effective numbers of electrons which participate to all possible transitions below the energy loss ΔE, and it will be convenient for the following discussion to compare these numbers for transitions induced either by the impact of photons :

$$\eta_{\mathrm{eff}}[\varepsilon_2(\Delta E)] = 7.67 \times 10^{-4}\,\frac{M_{\mathrm{at}}}{d} \times \int_0^{\Delta E} \Delta E.\varepsilon_2(\Delta E).\mathrm{d}(\Delta E)$$

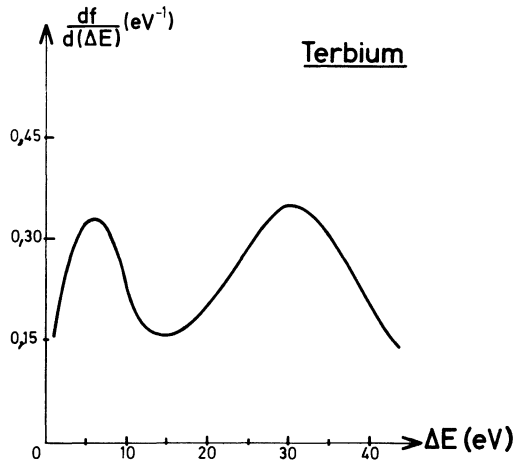

FIG. 9. — Spectral distribution of the optical oscillator strength for Tb.

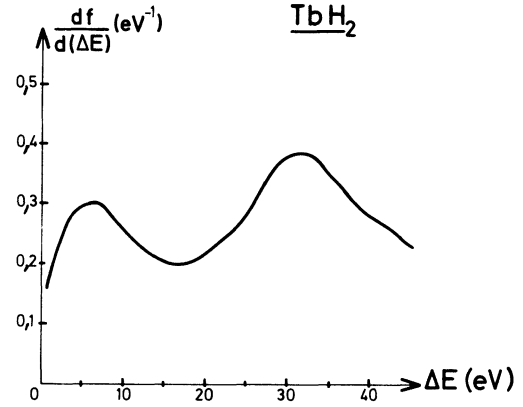

FIG. 10. — Spectral distribution of the optical oscillator strength for TbH_2.

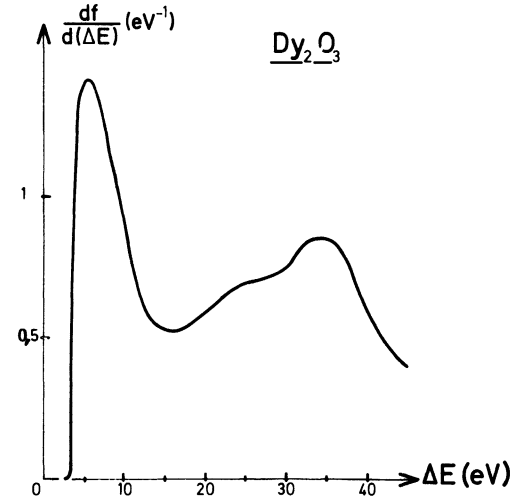

FIG. 11. — Spectral distribution of the optical oscillator strength for Dy_2O_3.

or by the impact of electrons :

$$\eta_{\text{eff}}\left[-\operatorname{Im}\frac{1}{\varepsilon}(\Delta E)\right] = 7.67 \times 10^{-4}\frac{M_{\text{at}}}{d} \times \times \int_0^{\Delta E} \Delta E\left(\operatorname{Im} - \frac{1}{\varepsilon(\Delta E)}\right) \mathrm{d}(\Delta E)\,.$$

In these formulae, ΔE is expressed in eV and these effective numbers are assigned respectively to one atom of terbium (Fig. 12), one molecule TbH_2 (Fig. 13) and one molecule Dy_2O_3 (Fig. 14).

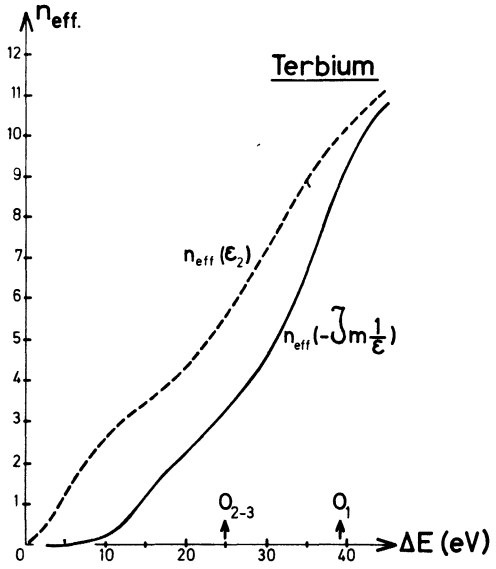

FIG. 12. — Effective number calculated for optical excitations $n_{\text{eff}}(\varepsilon_2)$ and for electron energy losses $n_{\text{eff}}\left(-\operatorname{Im}\frac{1}{\varepsilon}\right)$ for Tb.

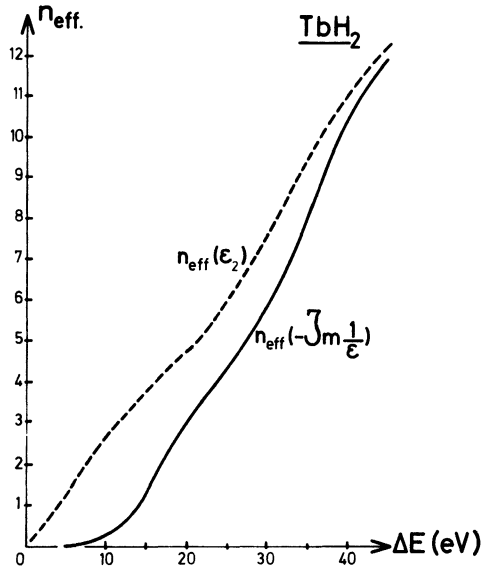

FIG. 13. — Effective number calculated for optical excitations $n_{\text{eff}}(\varepsilon_2)$ and for electron energy losses $n_{\text{eff}}\left(-\operatorname{Im}\frac{1}{\varepsilon}\right)$ for TbH_2.

We have carefully described the various steps of the calculation procedure that we have followed in order to give a more precise idea of the accuracy and limitations of this method. It is clear that the absolute values of the various computed coefficients are determined with a rather large uncertainty, which may be of the order of 20 % or more in some regions of the spectrum, especially in the low energy range ($\Delta E < 6$ eV). It should nevertheless be emphasized

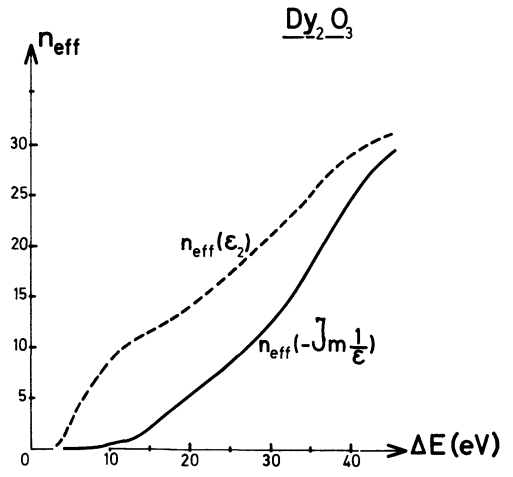

FIG. 14. — Effective number calculated for optical excitations $n_{eff}(\varepsilon_2)$ and for electron energy losses $n_{eff}\left(-\operatorname{Im}\frac{1}{\varepsilon}\right)$ for Dy_2O_3.

that this uncertainty remains comparable to that due to the impurities in the sample. The calculations are however sufficiently reliable for the following general discussion, the goal of which is not to extract rather precise data to be compared with optical measurements, but to obtain clearer information regarding the various contributions to the electron excitation spectrum in these solids.

4. **Discussion of the results.** — 4.1 PLASMON PEAKS. — The first structure lying generally between 10 and 16 eV can be attributed unambiguously to a collective excitation of the conduction (or valence) electron gas originating from the 6s and 5d atomic orbitals.

a) *Metallic plasmons.* — Our data concerning metals are in good agreement with Bakulin's values [3] for Ho, Er, Tm and Yb, but it appears that Daniels' measurements [4] on Gd and Dy have been carried out for areas composed of a mixture of various phases and not for pure metals. The plasmon energy value can be understood by assuming that there are 3 conduction electrons per atom participating to the collective excitation; however, with a lower $\hbar\omega_p = 9.7$ eV, ytterbium is confirmed to be divalent in the metallic state, which is inconsistent with recent assertions by Curzon and Singh [12]. In the framework of a free electron model, the experimental determination of the plasmon energy generally differs from the calculated value by a shift of 2 to 3 eV towards higher energies (see Table II). This difference is two or three times stronger than that noted for scandium and yttrium. How far can this effect be understood with the help of 4f electrons ? Such separations are generally interpreted by the occurrence of interband transitions (see for instance Daniels, Festenberg, Raether and Zeppenfeld [13]) : if they lie at lower frequencies, these transitions repel the plasmon energy towards higher values. Conversely, the interband transitions of higher energies lower the plasmon energy but the 5p shell in our case seems to lie too far above to have any strong influence. The analysis of our experimental data does not seem to reveal a strong influence of interband transitions from f levels towards vacant d states in the conduction band, for the dielectric constant ε_1 does not show any visible contribution $\delta\varepsilon_1$ of bound electrons excitations of the type

$$\sum_i \frac{f_i}{\omega_i^2 - \omega^2} \quad \text{with} \quad \omega_i \sim 7 \text{ eV}$$

(X-ray photoemission spectroscopy studies due to Heden, Löfgren and Hagström [14] would locate the major part of the filled 4f electronic states in terbium at about 7 eV under the Fermi level). Moreover, the first major contribution in the optical oscillator strength (Fig. 9) becomes exhausted at about 14 eV, which corresponds to $n_{eff}(\varepsilon_2)$ lying between 3 and 3.5 (Fig. 12). In conclusion, the oscillator strength associated with interband transitions from occupied f levels remains well below one electron per atom. This result is in good agreement with the reflectance studies on europium and ytterbium due to Endriz and Spicer [2] who conclude that there is little evidence for transitions from 4f-electron states either in anomalies in the structure of the optical conductivity or in increased oscillator strength. These authors suggest that the weakness of these transitions can be explained in terms of atomic like oscillator strengths following the theory of Fano and Cooper (15) and they conclude that the 4f → 5d-like state transition should account for less than 5 % of the total 4f oscillator strength (that is 0.5 electron/atom in Tb) : our results tend to confirm this assertion.

A closer examination of the plasmon peak in the energy loss function curve (Fig. 3) shows a maximum value of 1.5 for $\operatorname{Im}\left(-\frac{1}{\varepsilon(\Delta E)}\right)$ and a width at half-height of the order of 7 to 8 eV. Moreover, the profile seems to diverge from a Lorentzian curve because of longer tails on each side. All these characteristics express a rather weak screening by the metallic conduction gas as well as departures from the free electron model, which are not surprising in view of the partial d character of these conduction electrons.

b) *Collective excitations in hydrides* (LnH_2). — The plasmon peak in hydrides is generally shifted by some 3 eV above the position of the plasmon peak in the metal. This effect can be understood by assuming a higher density of *nearly free* electrons in the conduction band, originating from the hydrogen atoms : the discrepancy between the measured and the free-electron calculated values (with 5 electrons per molecule LnH_2) for the plasmon energy is similar in the metal and hydride phase (see Table II).

Electron energy band calculations by Switendick [16] show that for the dihydrides, an extra band corresponding to the antibonding combination of the two

TABLE II

Calculated values of plasmon energy in the free electron model : $\omega_p = \left(\frac{ne^2}{m\varepsilon_0}\right)^{1/2}$

	Plasmon peak positions (eV) exp	calc
Sc	14.0 ± 0.2	12.9
ScH_2	17.2 ± 0.5	15.9
Y	12.5 ± 0.2	11.2
YH_2	15.3 ± 0.5	14.0
Tb	13.3 ± 0.3	11.2
TbH_2	15.6 ± 0.5	13.6
Er	14.0 ± 0.3	11.6
ErH_2	16.8 ± 0.3	14.3

hydrogen 1s orbitals in the unit cell, is added below the Fermi energy. A determination of the plasmon energy value is not sufficiently sensitive to the details of the density of states curve in the neighbourhood of the Fermi energy to support this view of the band structure in rare earth dihydrides. Our calculated oscillator strength curve (Fig. 10) does not show any very noticeable effect below 17 eV where this contribution seems to vanish, except for a slower decrease, which is more clearly visible in the integrated curve $n_{eff}(\varepsilon_2)$ of figure 13. A value $n_{eff} \sim 4.5$ which, in the limits of the accuracy of our calculations, does not differ markedly from the free electron number 5, coincides with the exhaustion of the transitions from this conduction band. This contribution of the extra s electrons is also visible by a break in the slope of the ε_1 curve above 9 eV.

c) *Collective excitations in sesquioxides* (Ln_2O_3). — At first sight, the results concerning oxides spectra are not very different from those reported for metals and hydrides, except for Yb, in which case an important shift of the plasmon peak (peak « A » displaced from 9.7 eV to 17.0 eV) reveals a valence change of Yb ions from 2 to 3. For the other elements the plasmon energy value is intermediate between those for metals and hydrides and the shape of the corresponding peak is rather asymmetrical with a tail and secondary structures at higher energies. These experimental data are in very good agreement with those published by Bakulin [3] concerning Ho_2O_3, Er_2O_3 and Tm_2O_3.

It is obvious a *nearly free* electron model quickly fails in this case. We can interprete the plasmon energy value, in terms of the formula derived by Horie (17) : $\hbar\omega = [(\hbar\omega_p)^2 + E_g^2]^{1/2}$ where E_g is a typical value of the energy gap and $\hbar\omega_p$ is calculated in a free electron model with n_{eff} equal to the sum of all the electrons contained in the valence band. In order to evaluate the total number of occupied states in the valence band, it is equivalent to consider a simpler ionic model in which the lanthanide cations have transferred their electrons to the oxygen anions. In a cubic cell of C-Ln_2O_3 ($a \sim 10.5$ Å), there is therefore 288 valence electrons (48 oxygen atoms and 6-2p electrons per atom) leading to a theoretical value

$$\omega_p = \left(\frac{ne^2}{m\varepsilon_0}\right)^{1/2}$$

of the order of 20 eV for the plasma frequency, the influence of the gap width remaining quite negligible. This number is so large that such a model can only explain the experimental results by introducing a reduced n_{eff} of electrons per molecule Ln_2O_3 : the measured value of the plasmon energy for rare-earth oxides leads to an evaluation $n_{eff} \sim 12$ for a group Ln_2O_3.

To our knowledge, no band calculation seems to have been previously published concerning these substances, or the equivalent Sc_2O_3 or Y_2O_3 as far as the 4f electrons do not interfere in these excitations. We are therefore obliged to use only crude arguments and comparison with the situation of Ti_2O_3 and V_2O_3 which has been more thoroughly investigated (see, for example, the most recent calculations by Ashkenazi and Chuchem [18]).

The comparison of our calculated curves

$$-\operatorname{Im}\frac{1}{\varepsilon(\Delta E)} \quad \text{and} \quad \frac{df}{d(\Delta E)} \quad \text{for} \quad Dy_2O_3$$

leads to the following remarks.

(1) No attention must be paid to the structures below 6 eV because of the artificial extrapolation procedure that we have used in this energy range.

(2) The first absorption band involving the excitation of valence electrons is exhausted at about 15 eV, which is the energy value of the plasmon peak. When this energy value is carried back on the $n_{eff}(\varepsilon_2)$ curve, it corresponds to the excitation of a total number of 12 electrons per Dy_2O_3 molecule. This is in good agreement with the former determination of n_{eff} electrons involved in the collective excitation, following the quasi-free electron model.

(3) A second absorption band of weaker intensity lies between 15 and 27 eV. When integrated in the $n_{eff}(\omega_2)$ curve, the number of electrons involved in the excitations in this energy range is 18 − 12 = 6 electrons per Dy_2O_3 molecule. They seem to contribute to the asymmetrical profile of the plasmon peak and to the weak bump at 27 eV in the $-\operatorname{Im}\frac{1}{\varepsilon}$ function. It can be checked that this last feature cannot be interpreted as a double plasmon loss which has not been satisfactorily deconvoluted.

In their calculation of the band structure of Ti_2O_3 and V_2O_3, Ashkenazi and Chuchem show a schematic

diagram including the oxygen 2s and 2p bands and the transition metal 3d band. The 4s band which probably overlaps the upper part of the d band is thought to have only a minor effect. In these materials, the Fermi energy E_F is calculated to lie near the bottom of the d band, so that one d state in the Ti case and two d states in the V case are occupied. By extrapolation, no d state is occupied in Sc_2O_3 or in Ln_2O_3 so that the Fermi level falls in a forbidden gap, about 3 eV wide, between the bottom of the 5d conduction band and the top of the 2p oxygen band. The terminology used in the schematic band scheme of figure 15 is however somewhat misleading, for the binding in these oxides is not truly ionic but contains some admixture of covalency hybridization of metallic d states with oxygen orbitals. For example, Ashkenazi and Chuchem quote 7 % of 2p orbitals mixed in 3d band below the Fermi level in the conducting V_2O_3.

This valence band — labelled 2p in our scheme — lies between 3 and 8 eV below the conduction band and therefore contains 18 electrons per molecule. An other narrower valence band, originating mainly from the 2s oxygen states, is predicted to lie between 20 and 22 eV with 6 electrons per molecule (see Fig. 15).

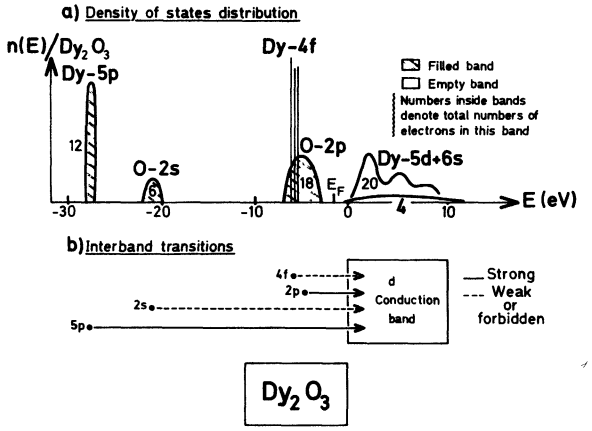

FIG. 15. — Simplified density of states curve for Dy_2O_3 with allowed and forbidden transitions in our model.

Our observed excitation spectra in Dy_2O_3 cannot be explained in terms of two groups of interband transitions issued from these two separated filled bands : the main argument comes from the absence of p symmetry in the empty conduction band, which must exclude the occurrence of interband transitions from the 2s states.

On the contrary, the strong d character of this conduction band which stretches over 10 eV or more, in heavy rare earth materials (as deduced from band calculations), must exhibit an important absorption band which represents the joint density of states of the filled 2p valence band and of the empty 5d-6s conduction band. The total width of this absorption band can therefore be of the order of 15 to 20 eV. A more detailed examination of the density of states distribution reveals strong variations characterized by a rather important d peak in the lower 4 eV of the conduction band [18]. The interband transitions originating from the 2p levels may also be separated into two fractions : a first one corresponds to transitions from 2p levels to these lowest d states of the conduction band, while another fraction may occur separately from the former and can be associated with transitions from low energy valence states to high energy conduction states. Moreover as Cazaux [19] demonstrated with the help of a Lorentz dielectric constant model, each one of these two types of interband transitions is followed by a plasmon-like peak in the electron energy loss function, situated respectively at 15 and 28 eV in the Dy_2O_3 spectrum, and corresponding to collective motion effects. This simple view of the experimental results can also explain the observed effective number values : all the electrons excited below 27 eV issue from the 2p valence band, partly below, partly above the 15 eV plasmon energy.

4.2 ABOUT THE 5p ELECTRON EXCITATIONS. — The second important contribution appearing through all our results in an energy range between 30 and 40 eV, is probably due to the excitation of the inner 5p electrons of the rare-earth ion. Several arguments support this interpretation. The position of this peak does not vary noticeably with the chemical state of the sample and moves continuously towards higher energies when increasing Z. It is located, above the O_{2-3} edge value determined by other experimental techniques [20]. Moreover, the effective number of electrons n_{eff} involved in excitation processes in this energy range, is always equal to six electrons per metallic ion. This contribution is visible as a strong absorption band in the oscillator strength curves or as a symmetrical peak, 10 to 12 eV wide, located about 10 eV beyond the threshold in the energy loss spectra. This behaviour is quite similar to the one which has been observed for scandium and yttrium [6] and for the first transition metals Ti or V [21, 22].

The coarse resemblance between the $\mathrm{Im}\left(-\frac{1}{\varepsilon}\right)$ and the $df/d\Delta E$ profiles in this energy range could reveal, in an individual transition model, some joint density of states distribution between a narrow (< 1 eV) inner 5p level and the unoccupied part of the conduction band, for symmetry arguments, which apply as well to the optical dipolar transitions and to small angle scattering electron excitations, favour such 5p to 5d transitions. Actually, the interpretation is a little more complex : it can be seen for example that the energy loss spectra also display some weak contribution located near the edge — the bump at 28 eV in figure 5 can be attributed in part to the occurrence of the first individual excitations from the 5p sub-shell, involving only an effective number of 1 electron per atom, before the development of strong-

er correlation effects in this shell responsible of the more intense delayed maximum.

The interpretation of the rather important shift of this structure above the edge together with its broadening, has been the goal of several works in the case of the transition metals, and similar calculations should be extended to the more complex situation of the rare-earth materials. We can in conclusion point out that the position of this maximum in the $df/d(\Delta E)$ curve lies generally a few eV (between 4 and 6) below the equivalent maximum in the energy loss function, while the ε_1 curve always displays a minimum at 35 eV which, without being a true pole responsible of a plasmon, suggests some collective behaviour. Without using a coarse « atomic plasmon » concept, we are thus lead to believe that the sudden creation of a 5p hole can be accompanied by a collective reorganization of the equivalent 5p electrons. (See Wendin [23] for an extensive discussion of similar effects.)

Acknowledgments. — We are very grateful to Dr. J. Frandon for fruitful discussions and communication of unpublished results.

References

[1] TREBBIA, P., COLLIEX, C., *8th Int. Conf. Electron Microscopy*, I, 382 Canberra (1974).
[2] ENDRIZ, J. G., SPICER, W. E., *Phys. Rev.* **B 2** (1970) 1466.
[3] BAKULIN, E. A., BALABANOVA, L. A., STEPIN, E. V., SHCHERBININA, V. V., *Sov. Phys. Solid State* **13** (1971) 189.
[4] DANIELS, J., *Opt. Commun.* **3** (1971) 13.
[5] BROUSSEAU-LAHAYE, B., FRANDON, F., COLLIEX, C., TREBBIA, P., GASGNIER, M., *Vacuum UV Radiation Physics* (Ed. E. Koch, R. Haensel, C. Kunz, Pergamon Vieweg) 1974, p. 622.
[6] BROUSSEAU-LAHAYE, B., COLLIEX, C., FRANDON, J., GASGNIER, M., TREBBIA, P., *Phys. Stat. Sol.* (b) **69** (1975) 257.
[7] GASGNIER, M., GHYS, J., SCHIFFMACHER, G., HENRY LA BLANCHETAIS, Ch., CARO, P. E., BOULESTEIX, C., LOIER, Ch., PARDO, B., *J. Less Common Met.* **34** (1974) 131.
[8] COLLIEX, C., TREBBIA, P., EMAG Conference, Bristol (1975), to be published in « *Advances in Electron Microscopy and Analysis* », Ed. J. Venables.
[9] TREBBIA, P., COLLIEX, C., *Phys. Stat. Sol.* (b) **58** (1973) 523.
[10] WEHENKEL, C., *J. Physique* **36** (1975) 199.
[11] KEIL, P., *Z. Phys.* **214** (1968) 251.
[12] CURZON, A. E., SINGH, O., *J. Less Common Met.* **39** (1975) 227.
[13] DANIELS, J., FESTENBERG, C. V., RAETHER, H., ZEPPENFELD, K., *Springer Tracts Mod. Phys.* **54** (1970) 77.
[14] HEDEN, P. O., LOFGREN, H., HAGSTROM, S. B. M., *Phys. Rev. Lett.* **26** (1971) 432.
[15] FANO, U., COOPER, J. W., *Rev. Mod. Phys.* **40** (1968) 441.
[16] SWITENDICK, A. C., *Int. J. Quantum Chem.* **5** (1971) 459.
[17] HORIE, C., *Prog. Theor. Phys.* **21** (1959) 103.
[18] ASHKENAZI, J., CHUCHEM, T., *Phil. Mag.* **32** (1975) 763.
[19] CAZAUX, J., *Opt. Commun.* **3** (1971) 221.
[20] BEARDEN, J. A., BURR, A. F., *Rev. Mod. Phys.* **39** (1967) 125.
[21] WEHENKEL, C., GAUTHÉ, B., *Phys. Stat. Sol.* (b) **64** (1974) 515.
[22] TREBBIA, P., Thèse de Spécialité, Orsay (1973).
[23] WENDIN, G., *Vacuum UV Radiation Physics* (Ed. E. Koch, R. Haensel, C. Kunz, Pergamon Vieweg) 1974, p. 225.